HETEROCYCLES, Vol. 85, No. 4, 2012, pp. 821 - 834. © 2012 The Japan Institute of Heterocyclic Chemistry
Received, 4th February, 2012, Accepted, 1st March, 2012, Published online, 6th March, 2012
DOI: 10.3987/COM-12-12439

SYNTHESIS, STRUCTURE, AND THEORETICAL CALCULATIONS OF A FURAN-BASED MOLECULAR WIRE, *N*-[4-(2-FURANYLMETHYLENEAMINO)BENZYLIDENE]FURAN-2-AMINE

Nathan C. Tice,[1]* Jennifer R. Armstrong,[2] Jeremy B. Maddox,[3] Sarah A. Ward,[3] Chad A. Snyder,[3] and Jason O. E. Young[3]

1. Department of Chemistry, Butler University, 4600 Sunset Avenue, Indianapolis, IN, 46208, USA, ntice@butler.edu

2. Department of Chemistry, Eastern Kentucky University, Richmond, KY, 40475, USA

3. Department of Chemistry, Western Kentucky University, Bowling Green, KY, 42101, USA

Abstract – The formation of the furanyl aryl imine *N*-[4-(2-furanylmethyleneamino)benzylidene]furan-2-amine (**1**) was accomplished by the condensation of furfural with 1,4-benzenediamine. The structure of the dimine **1** was confirmed by X-ray crystallographic analysis and displayed the expected, "zigzag" or *trans* conformation about the imine bond. Quantum chemistry calculations were carried out to model the electronic and molecular structure of **1** and to corroborate experimental characterizations.

Heterocycles and their fused-ring aromatic analogs represent an important class of organic compounds due to their applications in electronic materials, catalysis, medicine, and hydrodesulfurization (HDS) modeling.[1-6] Various heterocycles have been incorporated into conducting polymers and discrete monomers and oligomers, resulting in semiconducting properties when doped. Polythiophene and polypyrrole and their derivatives are most commonly employed due to their synthetic feasibility and high processibility.[7] In addition, polythiophenes have many practical advantages over other polymers, which include environmental stability and structural versatility.[8,9] Recently, many polymers and discrete heterocycle-containing molecules have been utilized in a wide varitey of real world applications,

including field-effect transistors (FETs), organic light-emitting diodes (OLEDs), and organic photovoltaic (OPV) cells.[10]

Although thiophenes and pyrroles have been most commonly studied for use in electronic devices, furans have been largely unexplored. Unlike thiophenes and pyrroles, furans can be derived directly and catalytically from biomass.[11,12] Some of these processes are intentional while others are seen as undesired by-products or major components in waste streams in the biorefinery sector. For example, the acid-catalyzed depolymerization and dehydration of cellulose from agricultural or forest activities produces furfural (Figure 1A). This industrial process is responsible for a yearly worldwide output of approximately 300,000 tons.[13] Furfural is also utilized for conversion to furfuryl alcohol (Figure 1B), which is a precursor to different types of resins and carbonaceous materials. Thus, furans represent an attractive, renewable feedstock for polymers, fibers, and other high-value materials. Furan derivatives have also shown a great deal of promise with respect to optical and electronic applications. For example, Zhang and coworkers found that incorporating isobenzofurans (IBFs) into conducting systems leads to materials with favorable electronic properties.[14] In other cases, the incorporation of furans led to materials with properties *superior* to those containing thiophenes. Meek and coworkers found that the use of IBFs over isothianapthenes (ITNs) led to improved dyes for near-infrared (NIR) fluorescence imaging.[15]

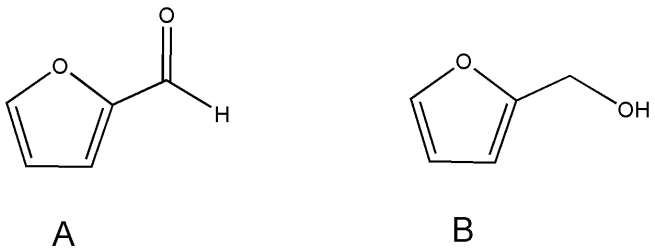

Figure 1. Furfural (**A**) and furfuryl alcohol (**B**)

One system that offers a great deal of promise in the area of novel electronic materials involves aromatic centers linked by conjugated units, known as "molecular wires." Many times these wires incorporate metallic centers to utilize their unique redox properties.[16] The metals themselves are said to be able to "communicate" electronically due the ability of charge to flow throughout the wire. We are primarily interested in forming novel molecular wire substrates for the eventual incorporation of transition metal centers using straightforward, low-cost routes. Specifically, the condensation of aldehydes with an aryl amine has found to be a facile pathway to bimetallic molecular wires. Imire and coworkers reported the formation of various biferrocene systems *via* the condensation of monoaldehyde ferrocene with aromatic diamines under mild conditions and high yields (Scheme 1).[17] We hoped to expand upon this novel synthesis and utilize building blocks derived from biomass. Herein, we report upon the formation, structure, and characterization of *N*-[4-(2-furanylmethyleneamino)benzylidene]furan-2-amine.

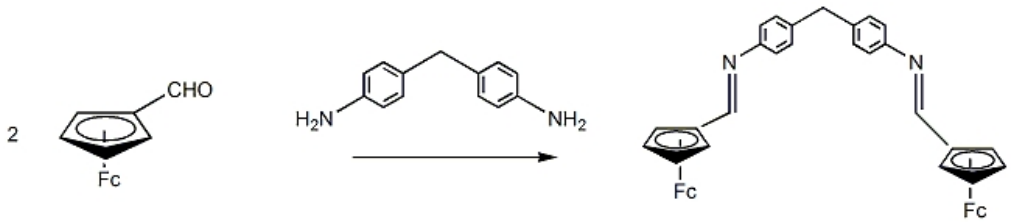

Scheme 1. Imire and coworkers route towards organometallic molecular wires

Our investigation into furan-based molecular wires involved the condensation of 1,4-benzenediamine (Scheme 2) with 2 equivalents of furfural. This is a well-known route, as a wide variety of furan condensation products, including our target wire, have been previously reported.[18] We varied the reaction conditions from reflux to 0 ˚C and reaction times from 2-24 hrs and found that optimized conditions for the formation of *N*-[4-(2-furanylmethyleneamino)benzylidene]furan-2-amine (**1**) involved stirring the reaction mixture in methanol for 2 hours at 0 ˚C. Compound **1** was isolated as a yellow solid as the filtrate from recrystallization of the crude product from methylene chloride and pentane in high yield (99%). Trials that utilized increased temperatures or longer reaction times adversely affected yield, although product formation was still reasonable in all cases (Table 1). These optimized conditions were similar to those that we previously found to be ideal in the condensation of methyl amine with ferrocenecarboxaldehyde.[19]

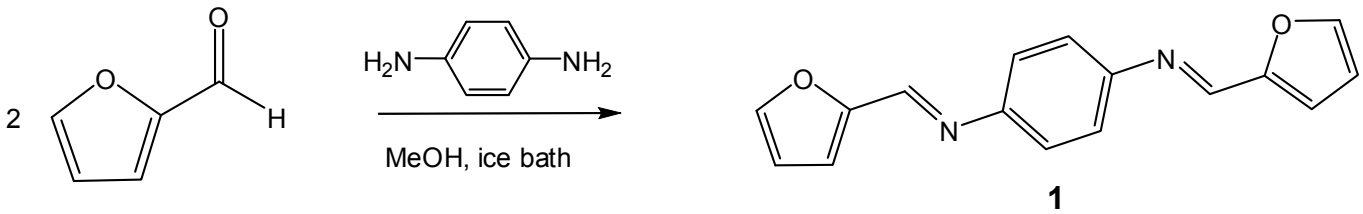

Scheme 2. Condensation trials of furfural with diaryl amines

Table 1. Trials for the formation of diimine **1**

Trial	furfural (mg)	1,4-phenylenediamine (mg)	Conditions	Yield (%)
1	250	140	reflux, 18 h	79
2	250	140	reflux, 6 h	80
3	250	140	room temp, 18 h	82
4	250	140	ice bath, 2 h	99

The air stable diimine **1** was soluble in a wide variety of organic solvents and could be handled and stored under ambient conditions for several months without noticeable decomposition. Compound **1** did

appear to be thermally unstable, as reflected in our observation of decreasing yields with harsher reaction conditions (higher temperatures, longer reaction periods). Significant decomposition was observed under the conditions in Trials 1-3, leading to lower isolated yields. The structure of the diimine **1** was confirmed by NMR, MS, and IR analysis. The ^{1}H NMR of compound **1** displayed the expected five signals: three for the furanyl groups (6.65, 7.08, and 7.78 ppm), one for the phenyl (7.30, broad singlet), and one for the imine protons (8.45 ppm). The ^{13}C NMR for **1** also displayed the imine resonance at 152.9 ppm as well as the disappearance of the carbonyl resonance from the starting material. Mass spectrometry confirmed the molecular weight of **1**, with both the base and molecular ion peaks at 264 m/z. IR spectroscopy displayed the typical aromatic ring and C-N stretching modes in the range 1450-1630 and loss of the carbonyl stretch from the aldehyde. Consistent with its thermal instability *in situ*, **1** also showed some decomposition in the solid-state at elevated temperatures. Both the melting point range (146.7-154.6 ˚C) and low carbon values observed *via* Elemental Analysis (70.30%, 72.72% calculated) for compound **1** also suggested thermal instability, and we attribute the results to such. The purity of compound **1** was confirmed by the absence of any anomalous signals in both its ^{1}H and ^{13}C NMR.

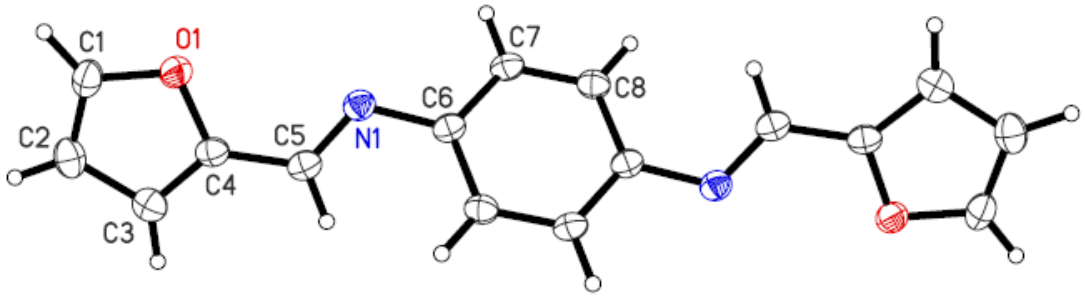

Figure 2. Molecular structure of **1** with 50% probability of ellipsoid plots

The structure of **1** was also confirmed by X-ray crystallographic analysis (Figure 2). Compound **1** crystallizes in a monoclinic, *P* 2_1/n space group, with 2 molecules in the unit cell. The structure for the diimine displays an inversion center within the central benzene ring. The molecule adopts a typical, "zigzag" or *trans* conformation along the imine (C5-N1) bond. Likewise, the furanyl rings adopt a highly planar, *trans* conformation with respect to each other, with the O1-C4-C5-N1 torsion angle measuring -5.4˚. In fact, the entire molecule is nearly planar, except for the torsion of the central benzene ring (C5-N1-C6-C7 torsion angle = 144.4˚), which provides the only deviation from planarity beyond 8˚. The aromatic nature of the furanyl rings is evident, with the C1-C2 and C3-C4 double bond lengths at 1.345 and 1.359 Å respectively. The greater single bond character for the C2-C3 and C4-C5 bonds is also evident, with bonds lengths at 1.418 and 1.431 Å, respectively. Conversely, the imine (C5-N1) bond is the shortest bond length observed in the structure of **1** at 1.2807 Å. Crystal data and a

summary of experimental details are given in Table 2. Tables of crystallographic details, atomic coordinates and displacement parameters, bond distances and angles, intermolecular contact distances, structure factors and a crystallographic information file (CIF) for the structure of **1** have been deposited with the Cambridge Crystallographic Data Centre.[20] General procedures and experimental data for **1** can be found in the references and notes section.[21]

Table 2. Crystal Data and Structure Refinement for compound (**1**)

Empirical formula	$C_{16}H_{12}N_2O_2$
Formula weight	264.28
Temperature	90.0(2) K
Wavelength	0.71073 Å
Crystal system	Monoclinic
Space group	$P\,2_1/n$
Unit cell dimensions a = 7.4730(2) Å b = 8.4137(3) Å c = 10.2570(3) Å	 $\alpha = 90^\circ$ $\beta = 90.003(1)^\circ$ $\gamma = 90^\circ$
Volume	644.91(3) $Å^3$
Z, Calculated density	2, 1.361 Mg/m^3
Absorption coefficient	0.092 mm^{-1}
$F(000)$	276
Crystal size	0.32 x 0.28 x 0.25 mm
θ range for data collection	2.73 to 27.48°
Limiting indices	-9<=h<=9, -10<=k<=8, -13<=l<=13
Reflections collected/unique	10507 / 1477 [R(int) = 0.0420]
Completeness to $\theta = 27.48$	99.5%
Absorption correction	Semi-empirical from equivalents
Max. and min. transmission	0.977 and 0.971

Refinement method	Full-matrix least-squares on F^2
Data / restraints / parameters	1477 / 0 / 91
Goodness-of-fit on F^2	1.019
Final *R* indices [I>2σ(I)]	*R*1 = 0.0450, *wR2* = 0.1185
R indices (all data)	*R*1 = 0.0617, *wR2* = 0.1313
Largest diff. peak and hole	0.209 and -0.240 e. Å^{-3}

To further characterize compound **1,** we have carried out a series of quantum chemistry calculations using the Gaussian 09 electronic structure package.[23] Starting with a molecular geometry extracted from the X-ray crystallographic structure, we have performed a ground state density functional theory (DFT) calculation using the Perdew, Burke, and Ernzerhof exchange and gradient-corrected correlation functionals[24] (PBEhPBE) with Dunning's correlation consistent basis sets[25] (both cc-pVDZ and cc-pVTZ).

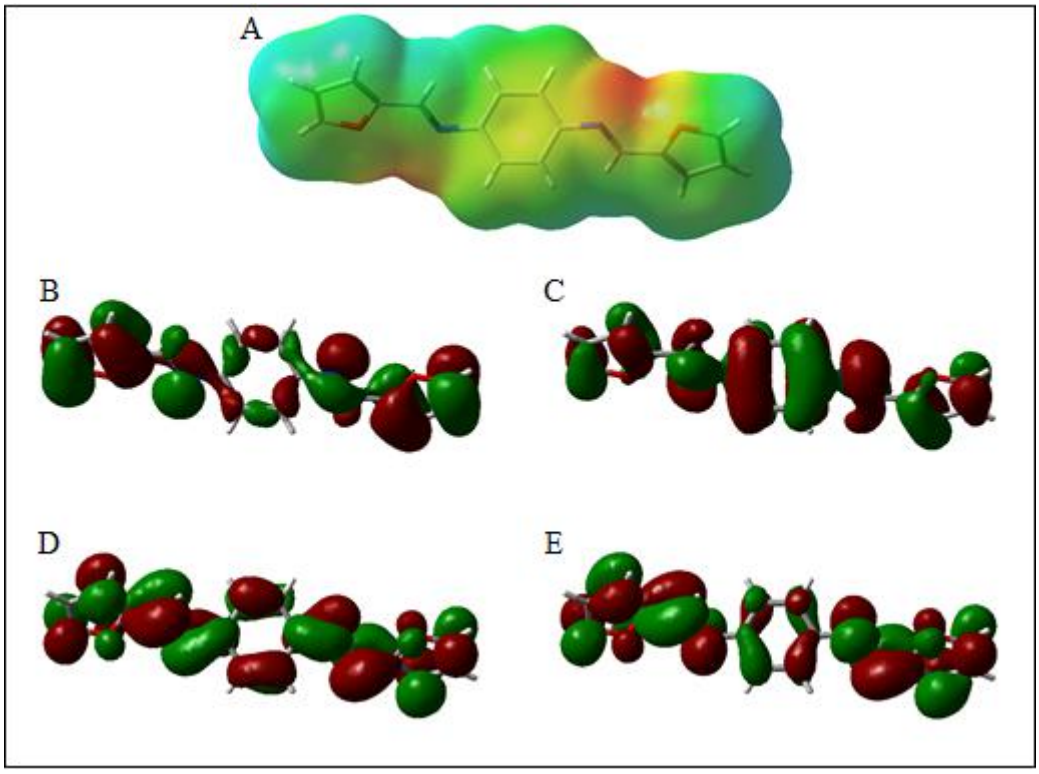

Figure 3. Calculated ground state electrostatic potential map and charge density (**A**), and selected molecular orbitals (**B-E**) for compound **1**. See text for details

Figure 3A shows the electrostatic potential (colors) mapped onto the ground state charge density (surface, isovalue = 0.004) as derived from a PBEhPBE/cc-pVTZ single point energy calculation. The red-yellow color indicates electron-rich regions near the imine bridge and furan oxygen atoms, while the blue-green color surrounding aromatic hydrogen atoms reflects more electron-deficient regions. The two highest energy occupied molecular orbitals, the HOMO-1 and HOMO, are shown in Figures 3B and 3C, respectively (surfaces, isovalues = 0.02). The HOMO-1 exhibits π bonding features within the furan rings; however, there is very little contribution from the central phenyl ring. The lobes on the imine group are in-plane and oriented away from the nitrogen atoms, which is characteristic of a lone pair or *n*-type (non-bonding) pattern. The HOMO has a characteristic π bonding pattern across the entire molecular back-bone with strong contributions on the central phenyl and imine groups. Figures 3D and 3E show the two lowest energy unoccupied molecular orbitals, the LUMO and LUMO+1, respectively (surfaces, isovalues = 0.02). The LUMO is representative of π* anti-bonding across the entire molecular back-bone, while the π* anti-bonding pattern for the LUMO+1 orbital is more intense on the furan and imine groups.

Table 3. Calculated excited electronic states, symmetries, transition energies, wavelengths, oscillator strengths, and NTO weights. Transitions to excited states 1 and 8 are the dominant electronic transitions

State	Sym.	Energy (eV)	Wavelength (nm)	Oscillator strength	NTO weights		
1	$\boldsymbol{A_u}$	**2.7676**	**447.98**	**0.8054**	**100**		
2	A_g	3.0234	410.08	0			
3	A_u	3.3351	371.75	0.0855	18	82	
4	A_g	3.3983	364.85	0			
5	A_g	3.6509	339.6	0			
6	A_u	3.743	331.24	0.0014	15	84	
7	A_u	4.011	309.11	0.1182	95		
8	$\boldsymbol{A_u}$	**4.1638**	**297.76**	**0.5041**	**37**	**56**	
9	A_g	4.2437	292.16	0			
10	A_u	4.2824	289.52	0.0364	26	73	
11	A_g	4.383	282.88	0			
12	A_u	4.4002	281.77	0.1811	12	37	51
13	A_g	4.6469	266.81	0			
14	A_u	4.66	266.06	0.0232	12	83	
15	A_g	4.7145	262.98	0			
16	A_u	4.7422	261.45	0.0089	100		

We have also performed a time-dependent density functional theory (TD-DFT) calculation for compound

1 using the PBEhPBE/cc-pVTZ model chemistry. Table 3 summarizes the predicted singlet-to-singlet electronic transitions with excitation energies below 4.7422 eV (or wavelengths greater than 261 nm). Due to the molecule's inversion symmetry (C_i point-group) these electronic transitions may be classified as either *gerade* (even) or *ungerade* (odd), and the *gerade* transitions are optically inactive due to symmetry cancellations. Among the active *ungerade* transitions, we identify two primary transitions with relatively large oscillator strengths that are expected to give rise to prominent bands in the optical spectrum.

We have performed a natural transition orbital (NTO) analysis[26,27] for compound **1** to help identify the nature of the dominant electronic transitions in our TD-DFT calculation. The lowest energy electronic transition at 2.77 eV (448 nm) has the largest oscillator strength (0.8504) among all the calculated electronic transitions, and would give rise to the leading band in the UV-visible spectrum. The NTO hole and particle for this transition are shown in Figures 4A and 4B, respectively, and there is only one dominant NTO hole/particle pair, i.e., these NTOs account for more than 99% of the electronic transition. The NTO hole and particle are remarkably similar to the HOMO and LUMO orbitals, respectively. In this case, the electronic transition may be attributed to the HOMO and LUMO, and it is very clearly a delocalized $\pi\rightarrow\pi^*$ transition, which is characteristic of the lowest energy transition for chain-like aromatic systems.

The second dominant electronic transition has a transition energy of 4.16 eV (298 nm), and there are two major NTO hole/particle pairs with significant contributions. The first hole/particle pair is shown in Figures 4C and 4D, respectively, and represents 37% of the transition. The NTO hole for this pair can be classified as π bonding within the central phenyl ring with negligible contribution from the furan rings, and it does not clearly resemble any single occupied orbital. The corresponding NTO particle is similar to the LUMO and has a π^* anti-bonding character. The second hole/particle pair is shown in Figures 4E and 4F, respectively, and carries a weight of 56%. The hole for this pair is also not directly connected with any single high-energy occupied orbital, and it appears that dominant contribution is π bonding localized to the furan rings and imine nitrogen atoms. The corresponding particle has a π^* character, and is also more or less localized to the imine and furan groups. We associate this electronic transition with a $\pi\rightarrow\pi^*$ transition within the furan ring-imine groups.

Figure 5 compares the theoretical electronic transitions (oscillator strength versus energy) with the experimental UV-vis spectrum of compound **1** in methylene chloride. The calculated transition energies are somewhat red-shifted compared to the two prominent low-energy peaks at 3.41 eV (364 nm) and 4.29 eV (289 nm), respectively. Nevertheless, there is a very good correspondence between the relative oscillator strengths of the calculated transitions and the observed peaks, and we can associate these features with the two dominant $\pi\rightarrow\pi^*$ transitions discussed above.

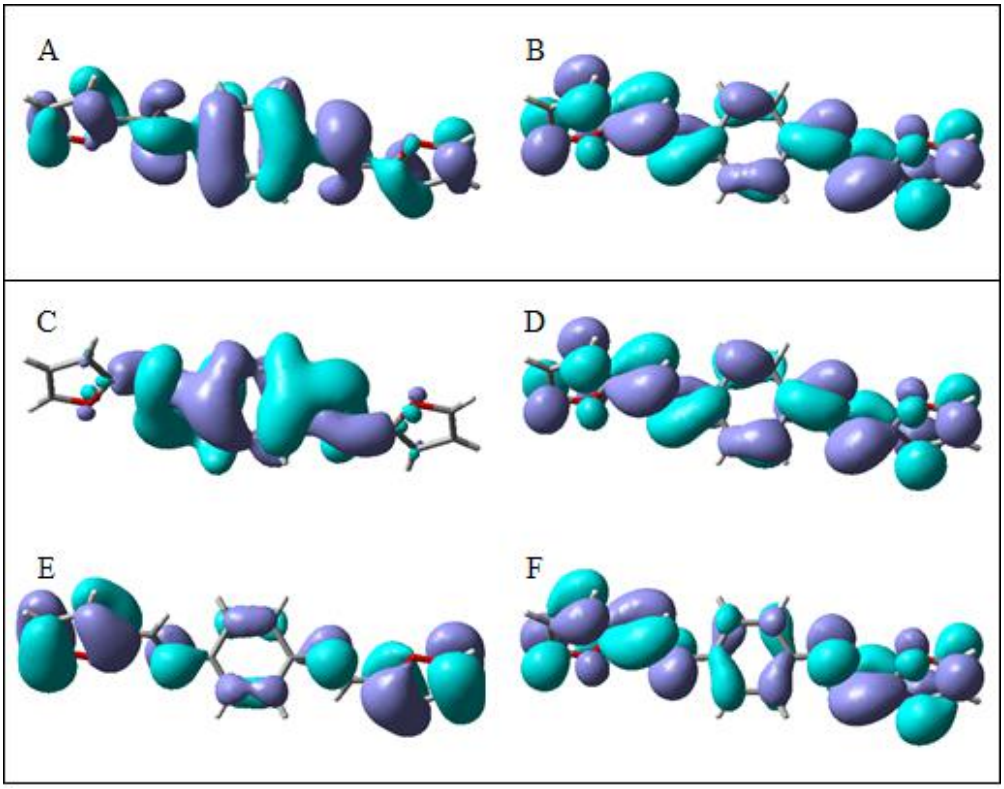

Figure 4. Calculated hole/particle natural transition orbitals (NTOs) for the dominant electronic transitions of compound 1. See text for details

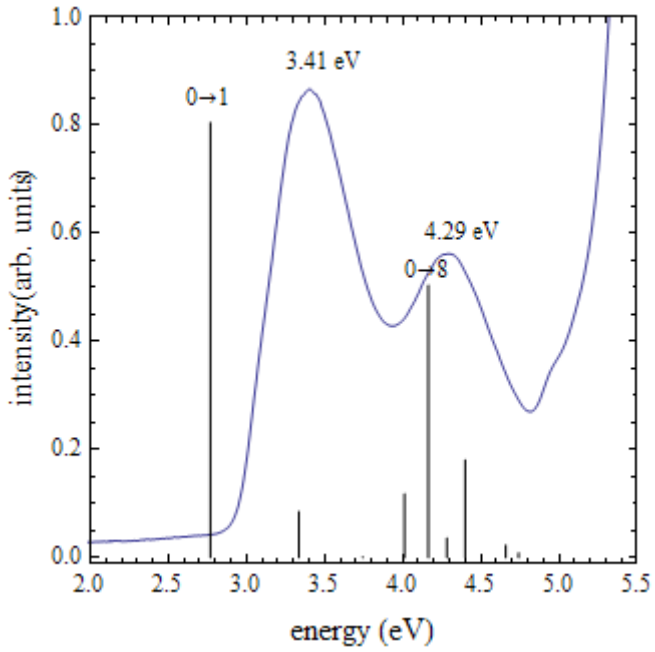

Figure 5. Comparison of calculated electronic transitions (vertical lines) with the experimental UV-vis spectrum (blue line) of compound **1** in methylene chloride. See text for details

We have also carried out a molecular geometry optimization (in vacuum) and normal modes analysis to identify and characterize the vibrational modes of compound **1**. These calculations were performed with the PBEhPBE/cc-pVTZ model chemistry using the crystal structure geometry as a starting point, and the molecule's inversion symmetry was enforced at each point along the optimization procedure. Comparison of the dihedral angles reveals that the optimized geometry of the molecule is slightly more planar than the crystal structure. The furan and the phenyl rings in both structures are nearly planar with all dihedral angles less than |±1˚|. The furan and imine groups are linked by the O1-C4-C5-N1 dihedral angle, and in both the crystal structure (-5.4˚) and optimized geometry (-2.1˚) the bridge is slightly non-planar. The C5-N1-C6-C7 dihedral angle linking the imine groups to the central phenyl ring is notably non-planar in both the crystal structure (144.4˚) and optimized (147.9˚) molecular geometries. The valance angles within the furan ring range from 106-111˚ in both the crystal and optimized structures, which are in agreement to within less than 1˚ for all angles. Similar agreement is found for the valence angles within the phenyl ring where the angles are between 119-121˚. There is a small 2.1˚ difference in the imine valence angle C5-N1-C6 and the optimized geometry (120.2˚) is slightly larger than the crystal structure angle (118.1˚). Overall, the crystal structure and optimized geometries are remarkably similar, which indicates that intermolecular interactions associated with the packing structure do not introduce significant strain within individual molecular units.

The predicted vibrational frequencies of compound **1** were determined to be within the experimentally established ranges for each functional group. A series of six C-H stretching modes for the furan rings were found with frequencies in the range of 3180-3200 cm^{-1}; three of these are weakly IR active and three are inactive due to symmetry. There are four C-H stretching modes associated with the phenyl ring between 3100-3122 cm^{-1}, and two of these are IR active. There are two C-H modes for the C5 bridge and one of these is strongly IR active at 2936 cm^{-1}. Finally, a very strongly IR active mode is predicted at 1617 cm^{-1} and corresponds to the C-N stretching. This is the most prominent and distinctive IR active mode among all the calculated vibrations within the molecular back-bone. The many remaining ring-stretching and breathing modes are much more convoluted across the backbone, and it is difficult to attribute these to any one particular sub-molecular unit.

It is important to note that the geometry optimization procedure discussed above finds only the nearest local minimum energy structure (for this particular model chemistry), which is not necessarily the global minimum energy structure. We have performed an additional conformational search by scanning the energy of compound **1** (at the PBEhPBE/cc-PVDZ level) with respect to the O1-C4-C5-N1 and C5-N1-C6-C7 dihedral angles, simultaneously, with strict enforcement of the molecular inversion symmetry. These calculations led to two low energy conformations, one *syn* and the other *anti* with respect to the O1 and N1 atoms.

Both structures were re-optimized at the PBEhPBE/cc-PVTZ level and a vibrational frequency analysis was performed to confirm that each structure is a local minimum. The *syn*-conformation is essentially the same as the optimized geometry derived from the crystal structure; however, there are slight differences (< 0.2°) between the dihedral angles. The O1-C4-C5-N1 and C5-N1-C6-C7 dihedral angles for the *anti*-conformation are 178.3° and 150.0°, respectively, such that the *anti*-conformer exhibits nearly the same degree of planarity, if not more so, compared to the *syn*-conformer.

Furthermore, we have used the synchronous transit-guided quasi-Newton (STQN) method[28] to locate a non-planar transition state between the *syn*- and *anti*-structures. The O1-C4-C5-N1 and C5-N1-C6-C7 dihedral angles for the transition state are -89.4° and 141.3°, respectively. Our calculations predict that the *anti*-type conformation is 6.11 kJ/mol (equivalent temperature is 752 K) lower in energy than the *syn*-type conformation. However, the energy barrier separating the *syn*- and *anti*-conformations is 86.39 kJ/mol (10,632 K) greater in energy than the *syn*-conformation, such that the *syn*-conformation, which is probably synthetically favored, is essentially locked into place.

Based upon these computational studies, the rigidity of the furyl-imine dihedral angle could be a potentially advantageous motif in the design of molecular wire structures. By this we mean that the placement of heteroatoms at specific sites within an aromatic system, such as the O1 and N1 atoms of compound **1**, could be useful for enforcing a particular molecular conformation that may favor a desirable opto-electric property. For example, the furyl-imine dihedral angle could possibly be used to control the spatial configuration of electron-donating or electron-withdrawing substituents on adjacent units within the molecular wire, and this could in turn be useful for tuning electronic couplings and transitions. In addition to the advantageous structural properties, the high yield and facile nature of its formation makes **1** an ideal candidate for bulk production in electronic materials applications. However, its apparent thermal instability might limit its real world practicality. Further studies on compound **1** in the solid state and its intermolecular properties and interactions will be necessary before fully evaluating its potential in an organic conducting material.

ACKNOWLEDGEMENTS

We would like to acknowledge our sources of funding for this project, including the Center for Renewable and Alternative Fuel Technologies and the Department of Chemistry at Eastern Kentucky University. We also wish to thank Dr. Sean Parkin at the University of Kentucky X-Ray Crystallographic Laboratories for his support on the solid state analysis. Additionally, we acknowledge the WKU Research & Creative Activities Program for its support as well as computer time and technical support from the WKU High Performance Computing Center.

REFERENCES AND NOTES

1. A. R. Katritzky and C. W. Rees, 'Comprehensive heterocyclic chemistry: structure, reactions, synthesis and uses of heterocyclic compounds,' Pergamon Press: Oxford, 1984.
2. P. Dallemagne, L. P. Khanh, A. Alsaidi, O. Renault, I. Varlet, V. R. Collot, R. Bureau, and S. Rault, *Bioorg. Med. Chem.,* 2002, **10**, 2185.
3. P. Dallemagne, L. P. Khanh, A. Alsaidi, I. Varlet, V. R. Collot, M. Paillet, R. Bureau, and S. Rault, *Bioorg. Med. Chem.,* 2003, **11**, 1161.
4. L. P. Khanh, P. Dallemagne, H. Landelle, and S. Rault, *J. Enzym. Inhib. Med.,* 2002, **17**, 439.
5. L. P. Khanh, P. Dallemagne, H. Landelle, and S. Rault, *Synthesis,* 2002, 1091.
6. M. Oh, J. A. Reingold, G. B. Carpenter, and D. A. Sweigart, *Coord. Chem. Rev.,* 2004, **248**, 561.
7. L. M. Tolbert, *Acc. Chem. Res.,* 1992, **25**, 561.
8. J. L. Bredas, A. J. Heeger, and F. Wudl, *J. Chem. Phys.,* 1986, **85**, 4673.
9. J. Roncali, *Chem. Rev.,* 1997**, 97**, 173.
10. J. E. Anthony, *Chem. Rev.,* 2006, **106**, 5028.
11. H. B. Zhao, J. E. Holladay, H. Brown, and Z. C. Zhang, *Science,* 2007, **316**, 1597.
12. Y. Roman-Leshkov, C. J. Barrett, Z. Y. Liu, and J. Dumesic, *Nature,* 2007, **447**, 982.
13. A. Gandini, *Macromolecules,* 2008, **41**, 9491.
14. H. Zhang, A. Wakamiya, and S. Yamaguchi, *Org. Lett.,* 2008, **10**, 3591.
15. S. T. Meek, E. E. Nesterov, and T. M. Swager, *Org. Lett.,* 2008, **10**, 2991.
16. For example see: J. J. Kim, S. U. Son, S. S. Lee, and Y. K. Chung, *Inorg. Chim. Acta,* 1998, **281**, 229; I. S. Lee, H. Seo, and Y. K. Chung, *Organometallics*, 1999, **18**, 1091; N. Szesni, M. Drexler, J. Maurer, R. F. Winter, F. de Montigny, C. Lapinte, S. Steffens, J. Heck, B. Weibert, and H. Fischer, *Organometallics,* 2006, **25**, 5774; M. Sato, T. Kitamura, T. Masiko, and K. Unoura, *J. Organomet. Chem.,* 2008, **693**, 247.
17. C. Imrie, P. Kleyi, V. O. Nyamori, T. I. A. Gerber, D. C. Levendis, and J. Look, *J. Organomet. Chem.,* 2007, **692**, 3443.
18. For example, see: M. E. Jamróz, M. Jarosz, J. Witowska-Jarosz, E. Bednarek, W. Tęcza, M. H. Jamróz, J. C. Dobrowolski, and J. Kijeński, *Spectrochim. Acta A,* 2007, **67**, 114; S. C. Ng, H. S. O. Chan, P. M. L. Wong, K. L. Tan, and B. T. G. Tan, *Polymer*, 1998, **39**, 4963; M. Mukhopadhyay, M. M. Reddy, G. C. Maikap, and J. Iqbal*, J. Org Chem.*, 1995, **60**, 2670.
19. N. C. Tice, S. Parkin, and J. P. Selegue, *J. Org. Met. Chem.,* 2007, **692**, 791.
20. CCDC 789472 contains the supplementary crystallographic data for this paper. These data can be obtained free of charge from The Cambridge Crystallographic Data Centre *via* www.ccdc.cam.ac.uk/data_request/cif.

21. **General Procedures.** All reactions were carried out using standard Schlenk techniques under a nitrogen atmosphere unless otherwise noted. NMR solvent acetone-d_6 and $CDCl_3$ (CIL) was used without further purification. Methanol, methylene chloride, pentane, furfural, and 1,4-benzenediamine (Aldrich) were also used without further purification.

^1H and ^{13}C NMR spectra were recorded on a JEOL-500 MHz NMR spectrometer at ca. 22 ˚C and were referenced to residual solvent peaks. All ^{13}C NMR spectra were listed as decoupled. Infrared spectra were recorded on Spectrum One FT-IR Spectrometer. Electron ionization (EI) mass spectra were recorded at 70 eV on a Perkin Elmer GC/MS or a Thermo Finnigan PolarisQ (quadrupole ion trap) at the University of Kentucky Mass Spectrometry Facility. Melting points were taken on a standard Mel-Temp apparatus. UV-Vis spectroscopy was performed on an Agilent 845x UV-Visible System. X-Ray diffraction data were collected at 90 K on a Nonius KappaCCD diffractometer at the University of Kentucky X-Ray Crystallographic Laboratories. Elemental analysis was performed at Atlantic Microlabs, Inc. in Norcross, GA.

Synthesis of *N*-[4-(2-furanylmethyleneamino)benzylidene]furan-2-amine (1): To a 100 mL round bottom flask, furfural (250 mg, 2.60 mmol) was added to a stirred solution of 1,4-benzenediamine (140 mg, 1.30 mmol) and 40 mL of MeOH in an ice bath. The reaction mixture was allowed to stir at 0 ˚C for 2 h and volatiles were removed under reduced pressure. The product was extracted with CH_2Cl_2 (30 mL) and the crude material was purified as the filtrate from a recrystallization from CH_2Cl_2/pentane, as a yellow solid (99%, 340 mg). Mp 146.7-154.6 ˚C. ^1H NMR (500 MHz, acetone-d_6, ppm): δ 6.65 (dd, 2H, $^3J_{AB}$ = 3.45 Hz, $^3J_{AC}$ = 1.7 Hz, OCHC*H*CH), 7.08 (d, 2H, ^3J = 2.85 Hz, OCHCHC*H*), 7.30 (br s, 4H, Ph), 7.78 (d, 2H, ^3J = 1.15 Hz, OC*H*CHCH), 8.45 (s, 2H, C*H*N). ^{13}C NMR (125 MHz, acetone-d_6, ppm): δ 108.0 (CH*C*HCH), 112.5 (*C*HCH*C*H), 112.8 (*C*CN), 125.3, 132.4, 146.3, 147.7 (Fr), 151.5 (C*C*N). ^{13}C NMR (125 MHz, $CDCl_3$, ppm): δ 112.3, 115.7, 121.9, 145.9, 147.4, 149.8 (Ar), 152.9 (N*C*H). IR (KBr, cm^{-1}): 3112 (CH-sp^2), 1627 (Ar). MS (EI, pos): 264 m/z (M^+ and base peak). Analysis for $C_{16}H_{12}N_2O_2$; Anal. Calcd: C, 72.72; H, 4.58; N, 10.60. Found: C, 70.30; H, 4.53; N, 10.82. Electronic spectrum (CH_2Cl_2) λ_{max} nm/(ε) 364 (483).

The X-Ray crystallographic structure of **1** was determined by X-Ray crystallographic methods. The crystals for which data were collected were typical of others in the batch, which had been grown by slow evaporation from methylene chloride at room temperature. These crystals were mounted on glass fibers with polyisobutene oil. Data were collected at 90 K on a Bruker KappaCCD diffractometer. The main programs used were DENZO-SMN to obtain cell parameters and for data reduction, SCALEPACK for scaling, merging and absorption correction, SHELXS-97 for structure solution, and SHELXS-97 for refinement.[22] Hydrogen atoms were placed in geometrically calculated

positions.

22. Z. Otwinowski and W. Minor, 'Methods in Enzymology, Macromolecular Crystallography,' Vol. 276, ed. by C. W. Carter Jr. and R. M. Sweet, Academic Press: New York, 1997.
23. Gaussian 09, Revision C.1, M. J. Frisch, G. W. Trucks, H. B. Schlegel, G. E. Scuseria, M. A. Robb, J. R. Cheeseman, G. Scalmani, V. Barone, B. Mennucci, G. A. Petersson, H. Nakatsuji, M. Caricato, X. Li, H. P. Hratchian, A. F. Izmaylov, J. Bloino, G. Zheng, J. L. Sonnenberg, M. Hada, M. Ehara, K. Toyota, R. Fukuda, J. Hasegawa, M. Ishida, T. Nakajima, Y. Honda, O. Kitao, H. Nakai, T. Vreven, J. A. Montgomery, Jr., J. E. Peralta, F. Ogliaro, M. Bearpark, J. J. Heyd, E. Brothers, K. N. Kudin, V. N. Staroverov, R. Kobayashi, J. Normand, K. Raghavachari, A. Rendell, J. C. Burant, S. S. Iyengar, J. Tomasi, M. Cossi, N. Rega, J. M. Millam, M. Klene, J. E. Knox, J. B. Cross, V. Bakken, C. Adamo, J. Jaramillo, R. Gomperts, R. E. Stratmann, O. Yazyev, A. J. Austin, R. Cammi, C. Pomelli, J. W. Ochterski, R. L. Martin, K. Morokuma, V. G. Zakrzewski, G. A. Voth, P. Salvador, J. J. Dannenberg, S. Dapprich, A. D. Daniels, Ö. Farkas, J. B. Foresman, J. V. Ortiz, J. Cioslowski, and D. J. Fox, Gaussian, Inc., Wallingford CT, 2009.
24. J. P. Perdew, K. Burke, and M. Ernzerhof, *Phys. Rev. Lett.*, 1996, **77**, 3865; J. P. Perdew, K. Burke, and M. Ernzerhof, *Phys. Rev. Lett.*, 1997, **78**, 1396; M. Ernzerhof and J. P. Perdew, *J. Chem. Phys.*, 1998, **109**, 3313.
25. T. H. Dunning Jr., *J. Chem. Phys.*, 1989, **90**, 1007.
26. During an electronic transition, the electronic density of a molecule rearranges in response to the applied radiation field. For some electronic transitions this process can be well-described by the promotion of an electron from a single occupied molecular orbital to a single unoccupied molecular orbital, and typically the lowest energy electronic transition involves the HOMO and LUMO. However, this picture can often be overly simplified, and in general, many occupied/unoccupied orbital pairs may significantly contribute to an overall electronic transition. In such cases, the so-called natural transition orbital (NTO) analysis[27] provides a mathematical prescription for transforming the canonical molecular orbitals in such a manner that the overall electronic transition can usually be represented by a smaller number (typically 1-3) so-called “NTO hole/particle pairs.” For a given electronic transition, the NTO holes represent the vacancy left behind after the charge density rearranges, and the corresponding NTO particles represent regions of space that are filled after the electronic transition. Graphical analysis of NTO can be used to elucidate the nature of electronic transitions.
27. R. L. Martin, *J. Chem. Phys.*, 2003, **118**, 4775.
28. C. Peng, P. Y. Ayala, H. B. Schlegel, and M. J. Frisch, *J. Comp. Chem*., 1996, **17**, 49.